

CHARACTERISTICS OF ULTRA-WIDEBAND ELECTROMAGNETIC MISSILE GENERATED BY FOCUSED TWO-DIMENSIONAL ARRAY

M. G. M. Hussain

Electrical Engineering Department
Kuwait University
P.O. Box 5969, Al-Safat 13060 Kuwait

Abstract—Ever since the concepts of “focus waves modes” and “electromagnetic missile” were introduced in the open literature almost two decades ago, extensive research work has been carried out to arrive at *physically realizable* applications for such concepts. In this paper, an ultra-wideband (UWB) electromagnetic missile with the time variation of a generalized Gaussian pulse (GGP) is generated based on the principle of focused-array beamforming. The radiation pattern, or array factor, of the focused-planar array is derived, and focused-energy patterns are computed to demonstrate the decaying behavior of the radiation energy of the electromagnetic missile as a function of distance travelled from the array to an observation point. The focused-energy patterns show that the depth-of-focus, or focusing bandwidth, is directly proportional to the focusing distance, and inversely proportional to the signal frequency bandwidth and array dimension. The focusing bandwidth is a measure of how well the energy is concentrated in the vicinity of the focusing point, and it is a useful parameter for radar ranging as well as imaging. In practice, the trade-off between the focusing distance, frequency bandwidth, and array dimension for improved focusing capability (or resolution) is of interest, in particular in the case of the ground-probing radar (GPR).

1 Introduction

2 Geometry of Focused Two-Dimensional Array

3 Ultra-Wideband Electromagnetic Missile

4 Radiation Energy of Electromagnetic Missile

5 Conclusions

References

1. INTRODUCTION

The origin of focused waves and Gaussian beam patterns is traceable to the pioneering work of DesChamps [1] and that of Brittingham [2]. According to the basic principle of antenna radiation, the power density of the infinitely extended periodic sinusoidal waves, and the energy density of finite duration signals, radiated by a radiator and propagating through a plane normal to the radiation axis decay like $1/r^2$, where r is the distance from the radiator to an observation point. In 1985, Wu [3] introduced the concept of *electromagnetic missile*, which is a propagating focused wave the energy of which decreases much more slowly than $1/r^2$; the energy decays as a function of $1/r^{2\epsilon}$, where ϵ is proportional to the rise time of the wave. The electromagnetic missile can also be represented as a propagating ultra-wideband (UWB) impulse of finite energy. The introduction of this concept marked the start of intensive research activities in the field of electromagnetic missile which has potential applications for radar, remote sensing, and medical diagnosis and imaging [4]–[14], [16]. The developing field of electromagnetic missile involves focused-array beamforming and transient-waveform design to achieve localized energy and desired (radiation) beam patterns. A brief history of the developments in this field and a comprehensive list of references can be found in [12].

In this paper, the characteristics of an electromagnetic missile and its associated energy patterns are derived and analyzed based on UWB electromagnetic pulses having the time variation of a generalized Gaussian pulse (GGP), radiated by a focused two-dimensional planar array. The GGP is a waveform model that closely represents the electromagnetic signals generated by an UWB impulse radiator [13], [14]. The energy spectral density of the GGP waveform is free from dc component; a condition required for the direct carrier-free emission of electromagnetic signals of finite energy.

In Section 2, the geometry of focused two-dimensional array of impulse radiators is described. In Section 3, the principle of focused two-dimensional array beamforming is presented and a focused wave, referred to as electromagnetic missile, is derived based on the GGP signal model. To show the characteristics of the propagating electromagnetic missile, its time variation at different observation points on and off the array axis are plotted. In Section IV, the radiation pattern, referred to as the array factor, for the focused two-dimensional array is derived. Also, energy patterns for the launched electromagnetic missile are derived and plotted for different design parameters. The plots show that the radiation energy of the

propagating electromagnetic missile peaks at the focusing point on the array axis, and then (slowly) decays as the travelled distance from the focusing point of the array increases. The rate at which the energy decays is inversely proportional to signal bandwidth and the dimension of the focused array.

Analogous to the concepts of range resolution and angular resolution, which are measured in terms of signal bandwidth and the half-energy beamwidth, respectively, a parameter referred to as *depth-of-focus* [15], or *focusing bandwidth*, is derived for the focused array and the GGP signal model. The focusing bandwidth of a focused array antenna provides a practical trade-off between array size, focusing distance, and signal bandwidth. Such a trade-off is essential in the case of ground-probing radar (GPR) for improving the depth-of-penetration into the ground and the resolution of subsurface images [16]. Conclusions are given in Section 5.

2. GEOMETRY OF FOCUSED TWO-DIMENSIONAL ARRAY

A two-dimensional square array of $M \times M$ elements is shown in Fig. 1. The array elements are uniformly spaced in the xz -plane with the separation distance d between any two adjacent elements. Each array element is an UWB impulse radiator, such as the *large-current radiator* described in [10], and it is denoted by R_{ij} , where $i = 0, \pm 1, \pm 2, \dots, m, j = 0, \pm 1, \pm 2, \dots, m$, and $M = 2m + 1$. The dimensions of the square array are of the length

$$D = 2md. \quad (1)$$

The element R_{00} at the center of the square array is referred to as the *reference element*. The location of any array element R_{ij} in the xz -plane, with respect to the reference element R_{00} , is determined by the *location vector* $\mathbf{d}_{ij} = \hat{x}(id) + \hat{z}(jd)$, where \hat{x}, \hat{y} , and \hat{z} are unit vectors in the $+x, +y$ and $+z$ axis directions, respectively. The array axis is aligned with the $+y$ axis. The *reference vector* \mathbf{r} from the reference element R_{00} to an observation point $P(r, \theta, \phi)$ in the wave zone is given by the relationship,

$$\mathbf{r} = \hat{x}(r \cos \theta \sin \phi) + \hat{y}(r \cos \theta \cos \phi) + \hat{z}(r \sin \theta). \quad (2)$$

In (2), $-90^\circ \leq \theta \leq +90^\circ$ is the elevation angle, and $-90^\circ \leq \phi \leq +90^\circ$ is the azimuth angle. The *distance vector* \mathbf{l}_{ij} from the element R_{ij} in the xz -plane to the observation point $P(r, \theta, \phi)$ equals

$$\begin{aligned} \mathbf{l}_{ij} &= \mathbf{r} - \mathbf{d}_{ij} \\ &= \hat{x}(r \cos \theta \sin \phi - id) + \hat{y}(r \cos \theta \cos \phi) + \hat{z}(r \sin \theta - jd). \end{aligned} \quad (3)$$

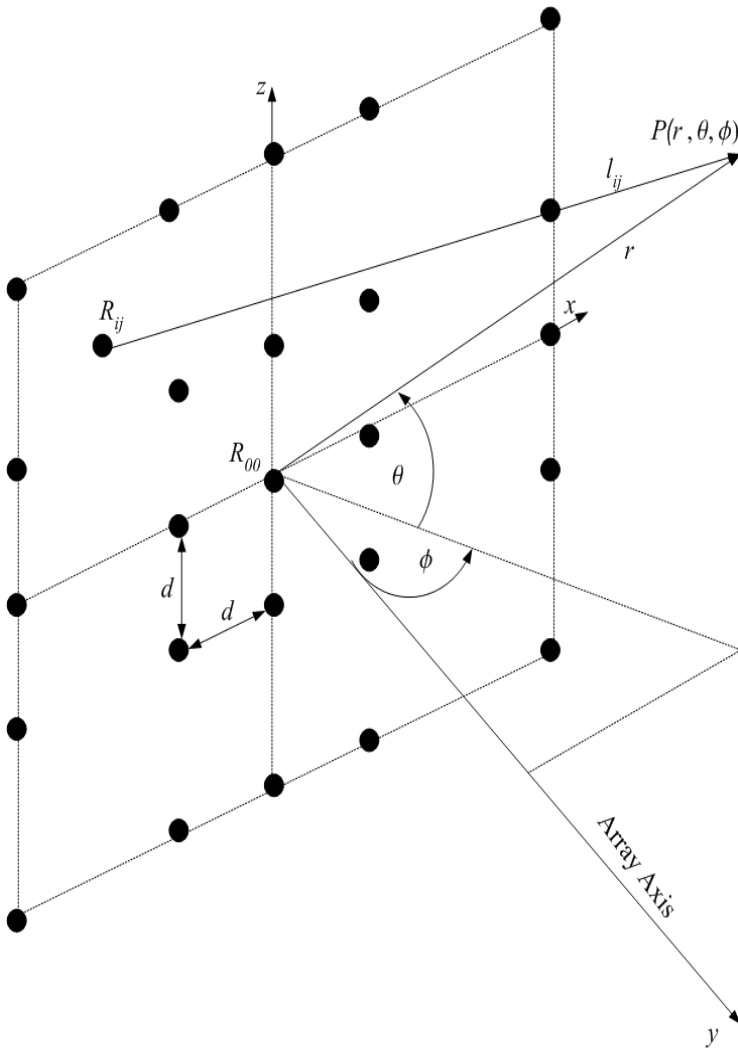


Figure 1. Geometry of two-dimensional square array of $M \times M$ elements uniformly spaced in the transverse xz -plane with a separation distance d between any two adjacent elements. Each array element is an impulse radiator denoted by R_{ij} , $\{i, j\} = 0, \pm 1, \pm 2, \dots, \pm m$; $M = 2m + 1$.

The relationship in (3) yields the magnitude of the distance vector

$$l_{ij}(r, \theta, \phi) = |\mathbf{l}_{ij}| = \left[r^2 - 2r(id \sin \phi \cos \theta + jd \sin \theta) + (id)^2 + (jd)^2 \right]^{1/2}. \quad (4)$$

A conventional phased-array antenna used for beamforming and electronic beamsteering with sinusoidal waveforms yields a radiation beam pattern defined in terms of θ and ϕ . A focused-array antenna provides a focused-energy pattern in the case of radiated signals, and a focused average-power pattern in the case of periodic sinusoidal waveforms, which show the decaying behavior of the radiation energy (or average power) of the propagating focus wave in terms of the travelled distance from the source. The planar square array in Fig. 1 can generate a focused wave by setting a proper delay time at each of the radiating elements R_{ij} so that the radiated signals will arrive simultaneously and sum coherently at the focusing point of the array. At any other position, the sum of the radiated signals will result in an out-of-focus, or a distorted, waveform whose time variation differs from that of the radiated signals.

For a focusing distance L from the reference radiator R_{00} at the center of the array in Fig. 1 to a focusing point $P(y = L, \theta = 0^\circ, \phi = 0^\circ)$ on the array axis, the (relative) focusing-delay time t_{ij} for the array element R_{ij} must be set according to the relationship

$$t_{ij} = L/c - \left[L^2 + (id)^2 + (jd)^2 \right]^{1/2} / c, \quad (5)$$

where c is the speed of light, $i = 0, \pm 1, \pm 2, \dots, \pm m$, and $j = 0, \pm 1, \pm 2, \dots, \pm m$. According to (5), the focusing-delay time $t_{00} = 0$ for the reference element R_{00} is the largest since the signal radiated by this element will experience the shortest propagation delay L/c to arrive at the focusing point $P(y = L, \theta = 0^\circ, \phi = 0^\circ)$ on the array axis. In this case, the array elements R_{ij} will radiate their excitation signals prior to the reference element R_{00} .

3. ULTRA-WIDEBAND ELECTROMAGNETIC MISSILE

A convenient signal model for representing a physically realizable UWB electromagnetic impulse whose energy density spectrum is free from dc component is the GGP signal with the time variation [13, 14],

$$\Omega(t) = E_o \sum_{k=0}^1 I_k \exp\{-a_k[(t - t_o)/\Delta T]^2\}, \quad (6)$$

where the coefficients I_k and a_k are defined as follows,

$$I_0 = 1/(1 - \alpha), \quad I_1 = -\alpha/(1 - \alpha), \quad \alpha \neq 1, \quad (7)$$

$$a_0 = 4\pi, \quad a_1 = 4\pi\alpha^2. \quad (8)$$

In (6), E_o is the peak amplitude at the time $t = t_o$, ΔT is a nominal duration, and α is a scaling parameter that shapes the energy density spectrum of the GGP signal. The Fourier transform of the signal $\Omega(t)$ results in the frequency spectral density function $\Lambda(f)$,

$$\begin{aligned} \Lambda(f) &= \int_{-\infty}^{+\infty} \Omega(t) \exp\{-j2\pi ft\} dt \\ &= \left(\frac{E_o}{2(1 - \alpha)\Delta f} \right) \exp\{-j2\pi t_o(f/\Delta f)\} \\ &\times \left(\exp\{-(\pi/4)(f/\Delta f)^2\} - \exp\{-(\pi/4\alpha^2)(f/\Delta f)^2\} \right), \quad (9) \end{aligned}$$

where $\Delta f = 1/\Delta T$ is the nominal frequency bandwidth. The energy spectral density of the signal $\Omega(t)$ is defined as $\Psi(f) = |\Lambda(f)|^2$, where $|\Lambda(f)|$ is the amplitude density spectrum.

The normalized time variation of the GGP signal $\Omega(t)$ and its energy density spectrum $\Psi(f)$ are shown in Fig. 2 for $t_o/\Delta T = 1$, and $\alpha = 0$ (dotted line), 0.75 (dashed line), 1.5 (dashed-dotted line), and 3 (solid line). For $\alpha = 0$, $\Omega(t)$ is an ideal Gaussian pulse whose energy density spectrum includes a dc component at $f = 0$; the plots for $\alpha \neq 0$ do not include a dc component.

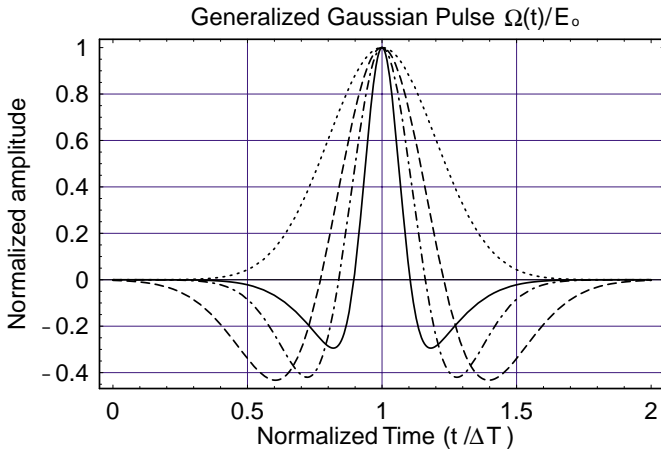
Let the GGP signal given in (6) be radiated by the focused square array in Fig. 1. The wave $s(t, r, \theta, \phi)$ arriving at the observation point $P(r, \theta, \phi)$ is the sum of the GGP signals radiated by the elements of the focused square array,

$$s(t, r, \theta, \phi) = \sum_{i=-m}^{+m} \sum_{j=-m}^{+m} \Omega(t - \tau_{ij}(r, \theta, \phi)), \quad (10)$$

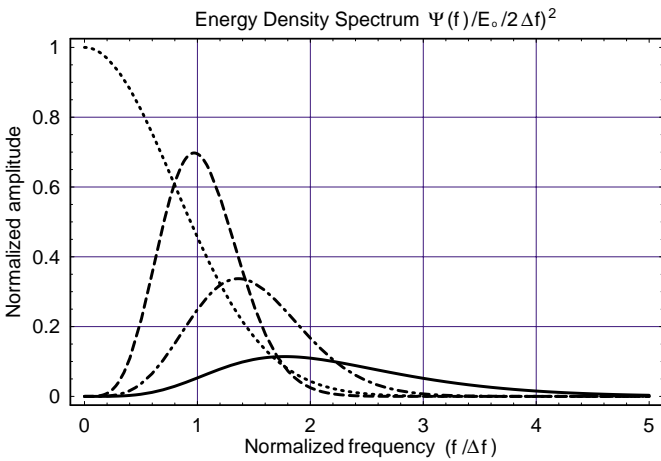
where $\tau_{ij}(r, \theta, \phi) = t_{ij} + l_{ij}(r, \theta, \phi)/c$ is the total delay experienced by the GGP signal radiated from the array element R_{ij} . With the help of (4), (5), and the substitutions

$$\rho = D/c\Delta T, \quad \xi = L/c\Delta T, \quad \zeta = r/c\Delta T, \quad (11)$$

the total delay time $\tau_{ij}(r, \theta, \phi)$ can be expressed by a normalized relationship that is more suitable for numerical computations as



(a)



(b)

Figure 2. Normalized time variation of the generalized Gaussian pulse $\Omega(t)/E_0$ (a), and its energy density spectrum $\Psi(f) = |\Lambda(f)|^2$ (b), for $t_0/\Delta T = 1$, and values of the scaling parameter $\alpha = 0$ (dotted line), $\alpha = 0.75$ (dashed line), $\alpha = 1.5$ (dashed-dotted line), and $\alpha = 3$ (solid line).

follows,

$$\begin{aligned}\tau_{ij}(\zeta, \theta, \phi) &= \tau_{ij}(r, \theta, \phi)/\Delta T \\ &= \xi + \rho \left[(\zeta/\rho)^2 - 2(\zeta/\rho)((i/2m) \sin \phi \cos \theta + (j/2m) \sin \theta) \right. \\ &\quad \left. + (i/2m)^2 + (j/2m)^2 \right]^{1/2} - \rho \left[(i/2m)^2 + (j/2m)^2 + (\xi/\rho)^2 \right]^{1/2}.\end{aligned}\quad (12)$$

The focused wave produced by the focused square array becomes

$$s(t, \zeta, \theta, \phi) = \sum_{i=-m}^{+m} \sum_{j=-m}^{+m} \Omega(t - \tau_{ij}(\zeta, \theta, \phi)\Delta T). \quad (13)$$

In (11), ρ is the normalized dimension of the planar array, ξ is the normalized focusing distance of the array, and ζ is the normalized reference range from R_{00} at the center of the focused array to any observation point $P(\zeta, \theta, \phi)$. The parameter ρ is also referred to as the *spacial bandwidth* of the focused array.

On the array axis where $\theta = \phi = 0^\circ$, the focused wave $s(t, \zeta, \theta, \phi) = s(t, \zeta)$ has the characteristics of an UWB *electromagnetic missile* whose energy is maximum at the focal point $P(\zeta = \xi, \theta = 0^\circ, \phi = 0^\circ)$ and decays in a fashion much more slowly than $1/\zeta^2$, as it propagates in the direction $\zeta > \xi$, away from the focal point of the focused array [3]. This phenomenon will be illustrated in the next section when we derive and plot various energy patterns of the focused array. With the help of (6) and (12), for $\theta = \phi = 0^\circ$, the UWB electromagnetic missile $s(t, \zeta)$ is expressed as follows,

$$s(t, \zeta) = \sum_{i=-m}^{+m} \sum_{j=-m}^{+m} \sum_{k=0}^1 E_o I_k \exp\{-a_k[(t - t_o)/\Delta T - \tau_{ij}(\zeta)]^2\}, \quad (14)$$

where the function $\tau_{ij}(\zeta)$ is given by

$$\begin{aligned}\tau_{ij}(\zeta) &= \xi + \rho \{ [(i/2m)^2 + (j/2m)^2 + (\zeta/\rho)^2]^{1/2} \\ &\quad - [(i/2m)^2 + (j/2m)^2 + (\xi/\rho)^2]^{1/2} \}.\end{aligned}\quad (15)$$

For a focused array with a large number of elements, $m \gg 1$, we may use the substitutions

$$\begin{aligned}u &= (i/2m), -1/2 \leq u \leq +1/2, \text{ for } -m \leq i \leq +m, \\ v &= (j/2m), -1/2 \leq v \leq +1/2, \text{ for } -m \leq j \leq +m,\end{aligned}\quad (16)$$

to approximate the two summations in (13) by two integrals,

$$s(t, \zeta, \theta, \phi) = (2m)^2 \int_{-1/2}^{+1/2} \int_{-1/2}^{+1/2} \Omega(t - \tau_{uv}(\zeta, \theta, \phi)\Delta T) du dv, \quad (17)$$

where the total delay is expressed in terms of u and v as follows,

$$\begin{aligned} \tau_{uv}(\zeta, \theta, \phi) = & \xi + \rho \left[(\zeta/\rho)^2 - 2(\zeta/\rho)(u \sin \phi \cos \theta + v \sin \theta) + u^2 + v^2 \right]^{1/2} \\ & - \rho \left[u^2 + v^2 + (\xi/\rho)^2 \right]^{1/2}. \end{aligned} \quad (18)$$

The waveform $s(t, \zeta)$ given in (14) is plotted in Fig. 3(a) and (b) for two observation points on the array axis: (a) $P(\xi, 0^\circ, 0^\circ)$, which is the focal point, and (b) $P(2\xi, 0^\circ, 0^\circ)$. Also, the waveform $s(t, \zeta, \theta, \phi)$ given by (13) is plotted in Fig. 3(c) and (d) for two observation points located in the focal plane but off the array axis: (c) $P(\xi, 0^\circ, 8^\circ)$, and (d) $P(\xi, 16^\circ, 0^\circ)$. The plots in Fig. 3 are calculated for the focused square array in Fig. 1 with 5×5 elements, normalized dimension $\rho = 5$, and normalized focusing distance $\xi = 2$. The radiated UWB signal from each array element is the GGP signal given in (6) with normalized delay $t_o/\Delta T = 1$ and scaling factor $\alpha = 3$.

According to Fig. 3, a focused signal having the exact shape as that of the radiated GGP signal shown in Fig. 2(a), but with larger peak amplitude, is generated at the focusing point $\zeta = \xi$ on the array axis. At any other observation point the generated signal is out-of-focus and distorted. The directional distortions associated with the waveforms in Fig. 3 convey information regarding range as well as angular coordinates and therefore have potential applications for UWB impulse radar [10–16], in particular, the ground-probing radar. Directional distortions cannot be observed in the case of periodic sinusoidal waveforms since the sum of sinusoidal functions with the same frequency will always yield a sinusoidal function with that frequency and possible amplitude and (ambiguous) phase variation. The fact that periodic sinusoidal waveforms have zero frequency bandwidth, they convey information at a rate equals zero too.

4. RADIATION ENERGY OF ELECTROMAGNETIC MISSILE

The radiation pattern of the focused square array in Fig. 1 is derived from the frequency spectrum of the focused signal given in (13) or (17). The Fourier transform of $s(t, \zeta, \theta, \phi)$ given in (13) results in the

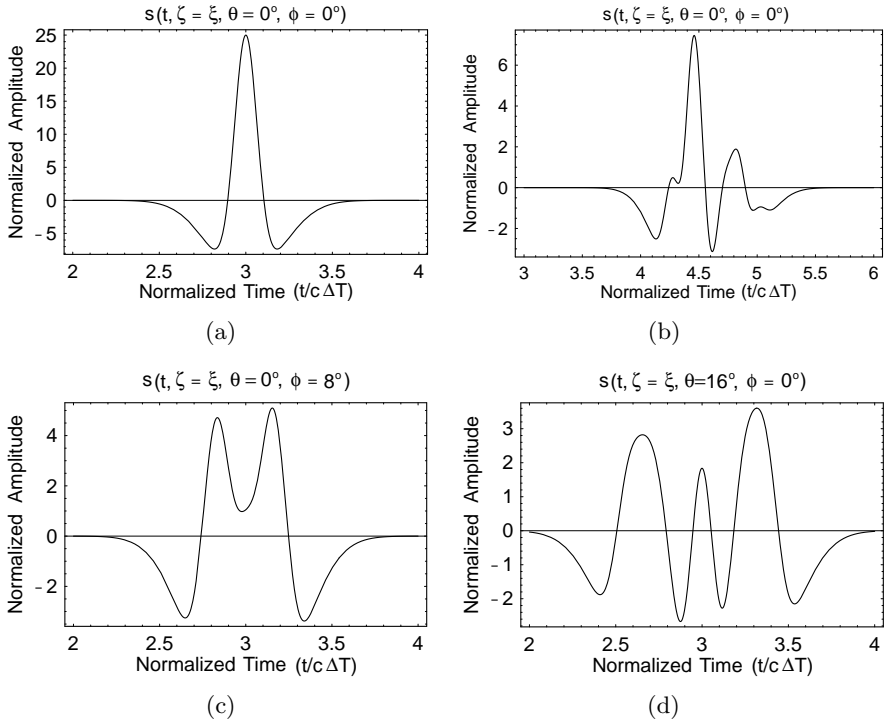


Figure 3. Time variation of the waveform $s(t, \zeta, \theta, \phi)$ generated at different observation points: (a) $P(\zeta = \xi, \theta = 0^\circ, \phi = 0^\circ)$, (b) $P(\zeta = 2\xi, \theta = 0^\circ, \phi = 0^\circ)$, (c) $P(\zeta = \xi, \theta = 0^\circ, \phi = 8^\circ)$, and (d) $P(\zeta = \xi, \theta = 16^\circ, \phi = 0^\circ)$. The plots are calculated for the focused square array in Fig. 1 with 5×5 elements, normalized focusing distance $\xi = 2$, spacial bandwidth $\rho = 5$. The radiated signal is the GGP signal given in (6) with scaling factor $\alpha = 3$ and normalized delay $t_o/\Delta T = 1$.

frequency density spectrum,

$$\begin{aligned}
 S(f, \zeta, \theta, \phi) &= \int_{-\infty}^{+\infty} s(t, \zeta, \theta, \phi) \exp\{-j2\pi ft\} dt \\
 &= \sum_{i=-m}^{+m} \sum_{j=-m}^{+m} \Lambda(f) \exp\{j2\pi f \tau_{ij}(\zeta, \theta, \phi)\}, \quad (19)
 \end{aligned}$$

where $\Lambda(f)$ is the frequency density spectrum given in (9). The integral of $S(f, \zeta, \theta, \phi)$ over the entire frequency bandwidth yields the radiation

pattern $F(\zeta, \theta, \phi)$ for the focused square array,

$$\begin{aligned}
 F(\zeta, \theta, \phi) &= \int_{-\infty}^{+\infty} S(f, \zeta, \theta, \phi) df \\
 &= \sum_{i=-m}^{+m} \sum_{j=-m}^{+m} \int_{-\infty}^{+\infty} \Lambda(f) \exp\{j2\pi f \tau_{ij}(\zeta, \theta, \phi)\} df. \quad (20)
 \end{aligned}$$

The integral in (20) is an inverse Fourier transformation that results in the function $\Omega[\tau_{ij}(\zeta, \theta, \phi)]$. Hence, the radiation pattern for the focused array becomes,

$$\begin{aligned}
 F(\zeta, \theta, \phi) &= \sum_{i=-m}^{+m} \sum_{j=-m}^{+m} \Omega[\tau_{ij}(\zeta, \theta, \phi)] \\
 &= \sum_{i=-m}^{+m} \sum_{j=-m}^{+m} \sum_{k=0}^1 E_o I_k \exp\{-a_k[\tau_{ij}(\zeta, \theta, \phi) - (t_o/\Delta T)]^2\}. \quad (21)
 \end{aligned}$$

Analogous to (17), for a large number of array elements $m \gg 1$, the radiation pattern can be approximated by two integrals,

$$\begin{aligned}
 F(\zeta, \theta, \phi) &= \int_{-1/2}^{+1/2} \int_{-1/2}^{+1/2} \sum_{k=0}^1 E_o I_k \exp\{-a_k[\tau_{uv}(\zeta, \theta, \phi) \\
 &\quad - (t_o/\Delta T)]^2\} du dv. \quad (22)
 \end{aligned}$$

The array factor is defined by the ratio,

$$A(\zeta, \theta, \phi) = \frac{F(\zeta, \theta, \phi)}{F(\xi, 0^\circ, 0^\circ)}. \quad (23)$$

where $F(\xi, 0^\circ, 0^\circ)$ is the largest value for the radiation pattern corresponding to the focal point $P(\xi, 0^\circ, 0^\circ)$ on the array axis.

The radiated energy contained in the signal $s(t, \zeta, \theta, \phi)$ is given by the integrals,

$$U(\zeta, \theta, \phi) = \int_0^{+\infty} [s(t, \zeta, \theta, \phi)]^2 dt = \int_0^{+\infty} |S(f, \zeta, \theta, \phi)|^2 df, \quad (24)$$

and the energy pattern of the focused array is defined by the ratio,

$$W(\zeta, \theta, \phi) = \frac{U(\zeta, \theta, \phi)}{U(\xi, 0^\circ, 0^\circ)}, \quad (25)$$

where $U(\xi, 0^\circ, 0^\circ)$ is the maximum signal energy concentrated at the focal point $P(\xi, 0^\circ, 0^\circ)$.

Based on (25), one may obtain various *energy patterns* for the focused square array in Fig. 1,

$$W(\zeta, \theta, \phi) = \begin{cases} W(\zeta), & \text{for } \zeta \geq \xi, \text{ and } \theta = \phi = 0^\circ, \\ W(\theta), & \text{for } \zeta = \xi, \text{ and } \phi = 0^\circ, \\ W(\phi), & \text{for } \zeta = \xi, \text{ and } \theta = 0^\circ, \end{cases} \quad (26)$$

where $W(\zeta)$ is referred to as the *focused-energy pattern*, $W(\theta)$ the *elevation-energy pattern*, and $W(\phi)$ the *azimuth-energy pattern*. The energy patterns $W(\theta)$ and $W(\phi)$ are the usual antenna patterns that one would derive in the case of conventional array beamforming, while the energy pattern $W(\zeta)$ represents the behavior of a focused wave, or an electromagnetic missile, as it propagates away from the source.

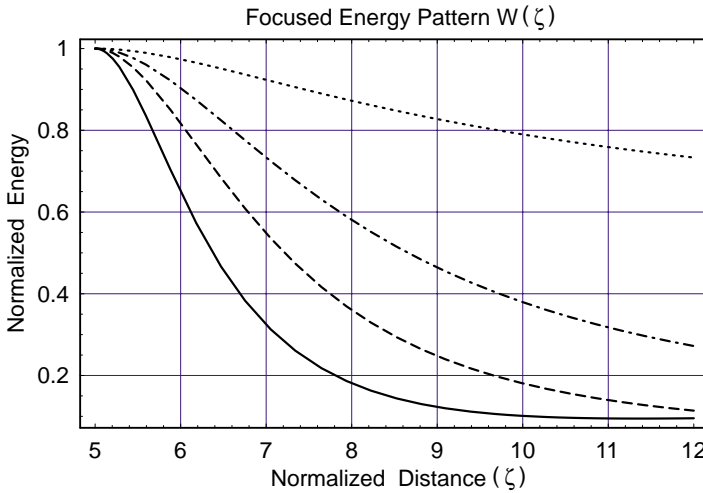


Figure 4. Focused-energy pattern $W(\zeta)$ for the focused square array in Fig. 1 with 5×5 elements, radiating GGP signals with $t_o/\Delta T = 1$, and scaling factor $\alpha = 0$ (dotted line), 0.75 (dashed-dotted line), 1.5 (dashed line), and 3 (solid line). The plots are computed for normalized focusing distance $\xi = 5$, $\theta = 0^\circ$, $\phi = 0^\circ$, and array spacial bandwidth $\rho = 5$.

The focused-energy pattern $W(\zeta)$ is shown in Fig. 4 for the focused square array in Fig. 1 with 5×5 elements, radiating GGP signals with $t_o/\Delta T = 1$, and scaling factor $\alpha = 0$ (dotted line), 0.75 (dashed-dotted line), 1.5 (dashed line), and 3 (solid line). The plots are computed for $\theta = 0^\circ$, $\phi = 0^\circ$, spacial bandwidth $\rho = 5$, and normalized focusing

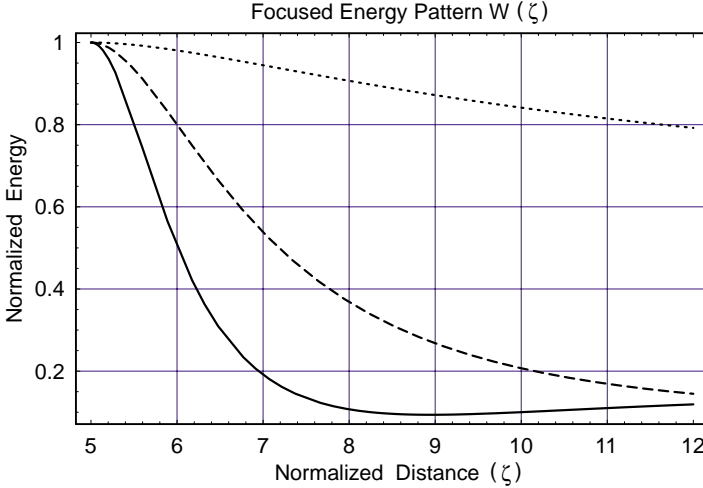


Figure 5. Focused-energy pattern $W(\zeta)$ for the focused square array in Fig. 1 with 5×5 elements, radiating GGP signals with $t_o/\Delta T = 1$, and scaling factor $\alpha = 3$. The plots are computed for array spacial bandwidth $\rho = 2$ (dotted line), 4 (dashed line), and 6 (solid line), $\theta = 0^\circ$, $\phi = 0^\circ$, and normalized focusing distance $\xi = 5$.

distance $\xi = 5$. The energy pattern represented by the dotted line is for an ideal Gaussian pulse with the scaling factor $\alpha = 0$.

The focused-energy pattern $W(\zeta)$ is also plotted in Fig. 5 for a fixed value of $\alpha = 3$, normalized focusing distance $\xi = 5$, and changing values of the spacial bandwidth $\rho = 2$ (dotted line), 4 (dashed line), and 6 (solid line).

According to Fig. 4 and Fig. 5, a large spacial bandwidth ρ for a focused array and a large scaling factor α (or frequency bandwidth Δf) for a radiated GGP signal yield a narrower focused-energy pattern $W(\zeta)$ with improved focusing capability. The focusing capability of a focused array antenna can be measured by a parameter referred to as *depth-of-focus* [15]. Analogous to the definition of the *moment of inertia* about a center of mass used in mechanics, the depth-of-focus $\delta_f(\xi)$ for the focused-energy pattern $W(\zeta)$ can be found by the relationship,

$$\delta_f(\xi) = \frac{\int_0^\infty (\zeta - \xi)^2 W(\zeta) (d)\zeta}{\int_0^\infty W(\zeta) (d)\zeta}. \tag{27}$$

The energy patterns in Fig. 4 and Fig. 5 show that in the vicinity of the focusing point $\zeta = \xi$, the depth-of-focus $\delta_f(\xi) \propto \xi/\alpha\rho$. Therefore,

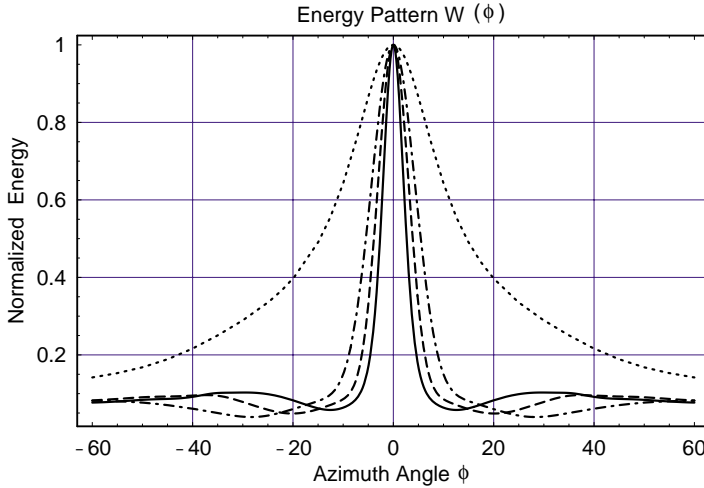


Figure 6. Azimuth-energy pattern $W(\phi)$ for the focused-planar array in Fig. 1 with 5×5 elements, radiating GGP signals with $t_o/\Delta T = 1$, and scaling factor $\alpha = 0$ (dotted line), 0.75 (dashed-dotted line), 1.5 (dashed line), and 3 (solid line). The plots are computed for the normalized focusing distance $\xi = 3$, the elevation angle $\theta = 0^\circ$, and array spacial bandwidth $\rho = 5$.

an approximation of (27) may be obtained from the relationship

$$\delta_f(\xi) \approx \frac{K\xi}{\alpha\rho} = \frac{KL}{\alpha D} = \frac{KL}{2m d \alpha}, \quad (28)$$

where K is a proportionality constant.

The azimuth energy pattern $W(\phi)$ is shown in Fig. 6 for the focused square array in Fig. 1 with 5×5 elements, spacial bandwidth $\rho = 5$, and normalized focusing distance $\xi = 3$. The plots are computed for GGP signals with $t_o/\Delta T = 1$ and scaling factor $\alpha = 0$ (dotted line), $\alpha = 0.7$ (dashed-dotted line), $\alpha = 1.5$ (dashed line), and $\alpha = 3$ (solid line). The azimuth energy pattern $W(\phi)$ in Fig. 7 is for a fixed value of $\alpha = 3$, $\xi = 3$, and increasing values of array spacial bandwidth $\rho = 2$ (dotted line), 4 (dashed line), and 6 (solid line). The larger the value of α and that of ρ the narrower the azimuth energy pattern $W(\phi)$, which yields improved angular resolution.

Due to the symmetry of the square array about the array axis, the elevation energy pattern $W(\theta)$ equals the azimuth energy pattern $W(\phi)$.

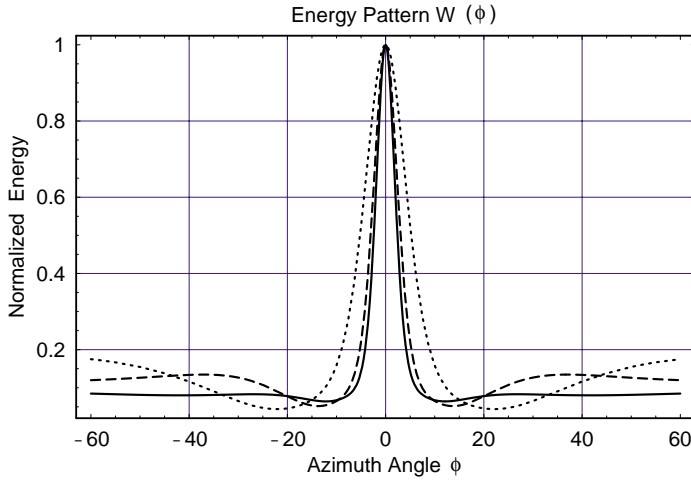


Figure 7. Azimuth-energy pattern $W(\phi)$ for the focused square array in Fig. 1 with 5×5 elements, radiating GGP signals with $t_o/\Delta T = 1$, and scaling factor $\alpha = 3$. The plots are computed for the normalized focusing distance $\xi = 3$, the elevation angle $\theta = 0^\circ$, and array spacial bandwidth $\rho = 2$ (dotted line), 4 (dashed line), and 6 (solid line).

5. CONCLUSIONS

The principle of two-dimensional-focused array for generating focused energy patterns was presented based on a physically realizable signal model. The time variation of the focused wave generated by the planar array is that of a generalized Gaussian pulse whose energy density spectrum is free from dc component. The radiation pattern, referred to as array factor, for the focused-planar array was derived as a function of array spacial bandwidth and the frequency bandwidth of the radiated GGP signal. Focused-energy patterns and azimuth energy patterns were plotted for different design parameters, e.g., spacial bandwidth, signal bandwidth, and focusing distance. The focused-energy pattern shows concentration of the radiated energy in the vicinity of the focusing point. The radiation energy decays in a fashion much more slowly than the inverse of distance squared as the focused wave propagates farther away from the focusing point on the array axis. This phenomenon corresponds to the propagation of electromagnetic missiles. The depth-of-focus derived for the focused-energy pattern is directly proportional to the focusing distance and inversely proportional to the array dimension and a scaling factor that controls the signal frequency bandwidth. A focused-planar array can

improve the performance of UWB impulse radar in general, and result in a deeper penetration depth for GPR.

REFERENCES

1. DesChamps, G. A., "Gaussian beam as a bundle of complex rays," *Electron. Lett.*, Vol. 7, 684–685, 1971.
2. Brittingham, J. N., "Focus waves modes in homogeneous Maxwell's equations: transverse electric modes," *J. Appl. Phys.*, Vol. 54, 1179–1189, 1983.
3. Wu, T. T., "Electromagnetic missiles," *J. Appl. Phys.*, Vol. 57, 2370–2372, 1985.
4. Heyman, E., B. Z. Steinberg, and L. B. Felsen, "Spectral analysis of focus wave modes," *J. Opt. Soc. Am.*, Vol. 4, 2081–2091, 1987.
5. Shen, H. M. and T. T. Wu, "The properties of the electromagnetic missile," *J. Appl. Phys.*, Vol. 66, 4025–4034, 1989.
6. Shen, H. M. and T. T. Wu, "The transverse energy pattern of an electromagnetic missile from a circular current disk," *SPIE O-E/LASE '89*, January 15–20, 1989.
7. Ziolkowski, R. W., "Localized transmission of electromagnetic energy," *Phys. Rev. A*, Vol. 39, No. 4, 2005–2033, 1989.
8. Ziolkowski, R. W., "Properties of electromagnetic beams generated by ultra-wide bandwidth pulse-driven arrays," *IEEE Trans Antennas and Propaga.*, Vol. 40, 888–905, 1992.
9. Hussain, M. G. M., "Ultra-wideband impulse radar — An overview of the principles," *IEEE Aerospace Electronic Systems Magazine*, Vol. 31, No. 9, 9–14, Sept. 1998.
10. Harmuth, H. F., R. N. Boules, M. G. M. Hussain, *Electromagnetic Signals: Reflection, Focusing, Distortion, and Their Practical Applications*, Kluwer Academic/Plenum, New York, 1999.
11. Hackett, R. D., C. D. Taylor, D. P. McLemore, H. Dogliani, W. A. Walton, III, and A. J. Leyendecker, "A transient array to increase the peak power delivered to a localized region in space: Part I — Theory and modeling," *IEEE Trans Antennas and Propaga.*, Vol. 50, No. 12, 1743–1750, December 2002.
12. Barrett, T. W., "Part 2: Energy transfer through media and sensing of the media," *Introduction to Ultra-Wideband Radar Systems*, J. D. Taylor (ed.), 365–434, CRC, Boca Raton, FL, 1995.
13. Hussain, M. G. M., "Principles of space-time array processing for ultrawide-band impulse radar and radio communications," *IEEE Trans. Veh. Technol.*, Vol. 51, No. 3, 393–403, May 2002.

14. Hussain, M. G. M., "Signal design for ultra-wideband radar and wireless communications," *Recent Advances in Simulation, Computational Methods and Soft Computing*, N. E. Mastorakis (ed.), WSEAS Press, 2002.
15. Rihaczek, A. W., *Principles of High Resolution Radar*, McGraw Hill, New York, 1969.
16. Hussain, M. G. M. and S. F. Mahmoud, "Energy patterns for a conducting circular disc buried in a homogeneous lossy medium and excited by ultra-wideband generalized Gaussian pulses," *Progress in Electromagnetics Research*, PIER 43, 59–74, 2003.

Malek G. M. Hussain was born in Kuwait in 1953. He received the Bachelor of Electrical Engineering, Master of Electrical Engineering, and Ph.D. in Electrical Engineering in 1977, 1979, and 1983, respectively, from the Catholic University of America, Washington DC, USA. In March 1977, he joined the Microwave Division of the Ministry of Communications in Kuwait and was awarded full scholarship in August 1977 for obtaining Master's and Ph.D. in the United States of America. In October 1983, he joined the Electrical Engineering Department at Kuwait University in the rank Assistant Professor. In May 1988, he was promoted to the rank Associate Professor and to the rank Full Professor in May 1993. From August 1988 to August 1989 he was Visiting Associate Professor at the Radiation Laboratory, Department of Electrical and Computer Science, University of Michigan, Ann Arbor, where he conducted research in the area of high-resolution ultra-wideband radar. In October 1991 he was appointed to the position Assistant Vice President for Research and Graduate Studies, and Director of Computer Services Center until May 1993. From June 1993 to August 1998, he was the Vice President for Academic Support Services. He is co-author of two books on propagation of carrier-free electromagnetic signals and their applications for radar and radio communications, and a contributing author to a book in the area of ultra-wideband radar systems. He is the recipient of the 2002/2003 Teaching Excellence Award, presented by the College of Engineering and Petroleum, Kuwait University. Also, he received the 1989 Kuwait Prize for the Advancement of Science, awarded by Kuwait Foundation for Advancement of Science.